Infiltration of Fibrous Preforms by a Pure Metal: Part V. Influence of Preform Compressibility

V.J. MICHAUD, J.L. SOMMER, and A. MORTENSEN

Infiltration by a pure matrix in the presence of preform deformation and partial matrix solidification is analyzed using a bounding approach for the preform rheology where solid metal is present. It is found, using parameters for the infiltration of short alumina fiber preforms by aluminum, that the two bounds are close in comparison to other factors of uncertainty in the prediction of infiltration rate. Using this approach, preform compression is shown to exert a significant influence on the infiltration rate for the system explored; in particular, the analysis shows the existence of an optimal value of applied pressure. Simplifications in the analysis are also presented, which yield fairly accurate results while easing their computation significantly.

I. INTRODUCTION

THE infiltration of a porous preform of reinforcing material by a liquid matrix material is one of the principal processes used in the production of metal matrix composites.[1,2] Physical phenomena which govern this process for an unalloyed matrix material were analyzed in previous publications of this series,[3–7] to show, in particular, that there can be a strong interplay in this process between liquid matrix flow and matrix solidification caused by initially low preform or mold temperatures.

It is generally assumed, in modeling infiltration, that the porous preform does not deform. In many practical cases, however, the liquid matrix is injected under high pressure to increase the rate of production of the composite and to overcome capillary forces which, particularly with metallic matrices, oppose infiltration and can leave residual porosity. These high pressures are transmitted to the preforms during infiltration and may, therefore, cause it to deform, influencing both the kinetics of the process and the structure of the composite thus produced. Since fiber preforms are relatively compliant porous materials, and since the applied pressure can be as high as 100 MPa, significant preform deformation is often observed in infiltrated composites.[8–23] In analyzing the infiltration process for these cases, preform deformation, then, cannot be neglected.

Composite infiltration processing is not the only practical situation involving flow of a liquid through a deformable porous medium: similar problems are found in biomechanics,[24–33] in magma mechanics,[34,35] and in soil mechanics, including groundwater hydrology, soil consolidation, and reservoir engineering.[36–41] Relevant physical laws are well established, having been presented in several articles[37–42] and confirmed by experimental studies.[43–47] In general, the formulation and solution of fluid flow through deformable porous media is complex, motivating the use of computer codes and the frequent introduction of various simplifying assumptions.[38,39,42,48–50]

Within this relatively large body of work, comparatively few authors have addressed the problem of infiltration of an initially dry deformable porous medium. Relevant work includes the analysis by J.R. Philip of unidirectional infiltration in swelling soils, which takes into account the effect of gravity and unsaturated flow and introduces the Boltzmann transformation in Lagrangian coordinates to treat the small-time limit, for which gravity effects can be neglected.[36] Other work includes unidirectional spontaneous infiltration experiments aimed at measuring the permeability of swelling soils[51,52] and numerical multidimensional analyses of two-phase flow and infiltration in deformable porous media.[53,54,55]

Sommer and Mortensen[56] recently proposed a treatment of infiltration of initially dry deformable porous media which, unlike previous analyses, is not restricted to small strains of the porous medium. This treatment neglects inertial forces as well as thermal and chemical transport phenomena and uses the slug-flow assumption, which assumes all infiltration to take place along a two-dimensional front within the preform. With this assumption, infiltration takes place at a single capillaric threshold pressure (ΔP_γ), which depends on the preform volume fraction, on the internal pore geometry, and on the wettability of the preform material by the liquid infiltrant. The slug-flow assumption has been shown to be justified in the infiltration of nondeforming porous media under sufficiently high applied pressure.[3–5,9,38,57] It was also shown in Reference 56 that an additional assumption, namely, the neglect of solid-phase velocity in favor of the average local liquid velocity, provides a considerably simplified method of treating the problem, which yields reasonably accurate results at moderate porous medium strains. This analysis was implemented fully for unidirectional infiltration under constant applied pressure using the Boltzmann transformation and was validated using experiments on the infiltration of a polyurethane sponge by ethylene glycol. A subsequent analysis along similar lines by Preciozi *et al.*[58] provided an evaluation of the effects of inertial forces and of variations in constitutive equations for the stress term.

V.J. MICHAUD and A. MORTENSEN, formerly with the Department of Materials Science and Engineering, Massachusetts Institute of Technology, Cambridge, MA 02139, are Research Scientist, Polymer and Composite Technology Laboratory, and Professor, Mechanical Metallurgy Laboratory, respectively, Materials Department, Swiss Federal Institute of Technology, Lausanne, CH-1015 Switzerland. J.L. SOMMER, formerly with the Department of Materials Science and Engineering, Massachusetts Institute of Technology, is Senior Research Scientist, Technical Research Associates, Salt Lake City, UT 84106-2379.

Manuscript submitted October 1, 1997.

As mentioned previously, in practical cases of metal matrix composite infiltration processing, partial matrix solidification often takes place within the preform during infiltration. Preform deformation and matrix solidification are, then, strongly coupled and cannot be analyzed separately using existing theory. Indeed, preform deformation alters the local volume fraction of reinforcing phase and, hence, the local extent of matrix solidification, while solid present within the matrix interferes with preform deformation; the two processes are, thus, interdependent. Experimental results so far indeed tend to indicate that solid metal can lock the preform in a compressed state, preventing it from relaxing both during and after infiltration.[21,22,59] This observation has motivated a few simplified treatments of the problem. In particular, Yamauchi and Nishida addressed the infiltration of a whisker preform under a steadily increasing pressure with no metal superheat. These authors assumed that solid metal formed during infiltration prevents further deformation of all portions of the preform once these are infiltrated; relatively good agreement with experimental results was obtained.[22]

We extend here the analysis developed in Reference 56 by using a bounding approach to address the adiabatic infiltration under constant applied pressure of a compressible fiber preform by a pure metal in the presence of matrix solidification caused by initially cold fibers. The bounding approach we adopt is motivated by the fact that the exact rheological behavior of the preform in the presence of a partly solid matrix will generally remain unknown, given the microstructural complexity of the three-phase material at hand and the complex time-dependent behavior expected of solid metals at their melting point. This approach is, furthermore, justified by results obtained *in fine*, namely, that, under practical circumstances, the two bounds are quite close for systems of engineering relevance.

The bounds we consider represent a lower and an upper bound for the kinetics of infiltration corresponding, respectively, to the upper and lower bounds for the rigidity of the infiltrated preform in the presence of solid metal. The lower bound assumes that the presence of solid metal prevents all local deformation of the preform once infiltrated (as was assumed by Yamauchi *et al.*), while the upper bound assumes that solid metal has no effect at all on preform relaxation during infiltration.

In what follows, we first treat the simpler case for which the metal has no superheat, and show, for a case of practical interest, that the two bounds are close, *i.e.*, within the range of generally observed experimental error. We then compare the results of the upper-bound calculations to those obtained using the simplified treatment proposed in Reference 56. We finally investigate the effect of metal superheat, considering again the two bounds and assuming that the preform is fully relaxed in the remelted zone.

II. GENERAL STATEMENT OF THE PROBLEM

A. *Assumptions*

We consider the unidirectional infiltration of a porous preform, initially at a temperature T_f and containing gas at pressure P_g, by liquid metal, which is injected under a constant pressure P_o and at temperature T_o at one end of the porous medium. We assume that the porous medium is fixed at its other far end. Both flow and preform deformation take place only along the x direction. All assumptions concerning fluid flow and capillarity follow closely those of Reference 56 (the terminology used here differs, however, somewhat from that in Reference 56, for consistency with previous articles of the present series[3–6]). In particular, we use the slug-flow assumption and estimate the capillary pressure ΔP_γ, which must be overcome for full infiltration of pores, as[60]

$$\Delta P_\gamma = -S_f \sigma_{LA} \cos(\theta) \qquad [1]$$

where θ is the contact angle of the liquid metal on the flat solid substrate material, σ_{LA} is the liquid matrix surface energy, and S_f is the total surface area of solid/liquid interface per unit volume of the liquid matrix in the infiltrated porous material.

We consider the porous medium to be a continuum and define the local volume fraction of solid phase, including solid metal formed during infiltration, as $V_{sf} = V_f + V_s$, where V_f is the local fiber volume fraction, and V_s is the volume fraction of solid metal formed, if any. Where liquid is present, its volume fraction is, thus, everywhere $(1 - V_{sf})$. We assume that the system is adiabatic and that heat exchange between fibers and metal takes place, within a representative volume element ΔV, rapidly compared to the time for overall preform infiltration; hence, the temperature T can be considered uniform within ΔV. Also, we assume that any solid metal formed moves together with the fiber and, hence, attribute only one velocity to all solid within ΔV. We take the thermal properties of the fiber preform and of the liquid metal to be independent of temperature, the solid and liquid metal densities to be equal, and neglect heat transfer in the noninfiltrated preform. All these assumptions have been shown to be justified for infiltration of nondeformable preforms.[3,4]

We neglect all body forces, including gravitational forces. This assumption is valid when pressure gradients within the infiltrated portion of the porous medium are larger than the sum of all body forces in the fluid (this is generally the case, in practice). We also neglect inertial forces, both within the preform and within the flowing liquid, in favor of viscous forces at the boundary between the liquid and solid phases; as a corollary, fluid flow follows Darcy's Law. We assume that the porous medium is isotropic in a plane perpendicular to the x-axis, such that the infiltration direction is a principal direction of the preform permeability tensor.

B. *General Description of the Problem*

Writing $P_o = \Delta P_T + P_g$, we define the pressure differential ΔP_T, which drives flow of the fluid into the preform. It is this pressure differential, transmitted to the preform by the fluid, which causes deformation of the porous solid medium during infiltration. This deformation is, in turn, dependent on the intrinsic rheology of the porous solid preform. In the configuration (unidirectional infiltration) of present interest, this rheology is characterized by the stress-strain curve measured on a dry sample of the porous medium in a unidirectional compression test with no strain transverse to the loading direction. For porous ceramic preforms used in the fabrication of composite materials, this curve generally has the form depicted in Figure 1(a), drawn

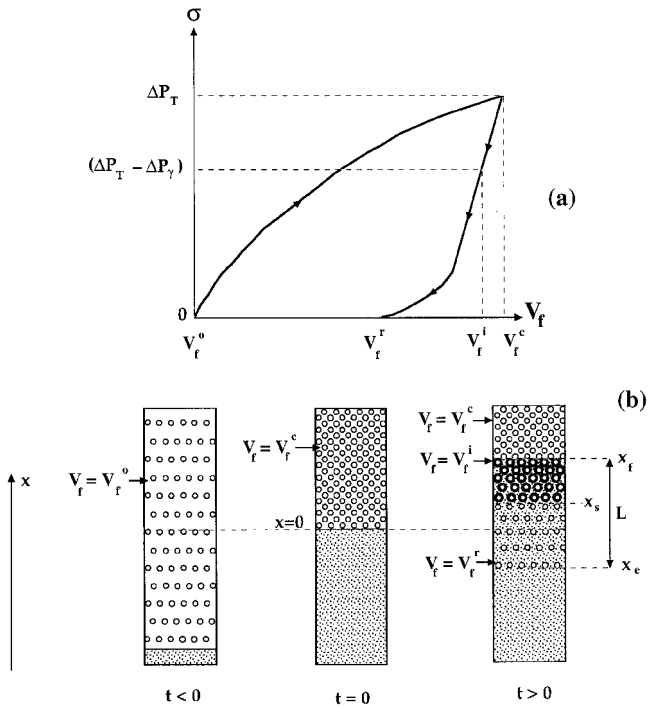

Fig. 1—(*a*) Schematic illustration showing the uniaxial compression behavior of a dry porous solid during infiltration by a nonwetting liquid under a constant applied pressure ΔP_T. (*b*) The same solid before and during nonisothermal infiltration by a nonwetting superheated liquid under a constant applied pressure ΔP_T.

for loading to ΔP_T and unloading to zero stress, using the fiber volume fraction instead of strain for the horizontal axis. Barring chemical interaction between the infiltrant and the preform, the stress-strain behavior of the preform is not affected by the presence of fluid if the latter can flow freely out of the pores and has a low viscosity.[61] When solid metal is present, however, the preform may well exhibit a highly different mechanical behavior than when it is dry.

In the very first instant of contact between the liquid and the preform, there is a transient period during which the liquid is decelerated by the porous medium. Simultaneously, the preform is rapidly compressed to a volume fraction of $V_f = V_{fc}$, the preform volume fraction corresponding to $\sigma = \Delta P_T$ on the stress–volume fraction curve (Figure 1(a)). As in Reference 56, we do not consider the dynamics of this initial transient and simplify the problem by assuming compression of the porous material to be instantaneous at $t = 0$ and Darcy's law to be valid throughout infiltration. At the time $t = 0$, the infiltration front is then located precisely at the entrance of the porous preform compressed under the full applied pressure ΔP_T (Figure 1(b)). Using a Eulerian x-axis that remains fixed in relation to the uninfiltrated portion of the preform and that is oriented along the direction of infiltration, we define $x = 0$ as this common location of the preform entrance and infiltration front at $t = 0$.

Where liquid is present, deformation of the preform is governed by the *effective* stress σ, which, in this system of relatively low solid-phase percolation (since compressible preforms are generally made of stacked discrete solid elements such as fibers or particles), equals the total stress acting on ΔV minus the fluid pressure P.[46,55,62–64] At $t > 0$, therefore, as the infiltration front traverses the preform, the effective stress jumps from $\sigma = P_o - P_g = \Delta P_T$ ahead of the infiltration front to $\sigma = \Delta P_T - \Delta P_\gamma$ right behind the infiltration front. The preform strain then decreases to the value V_f^i given by the unloading stress–volume fraction curve in Figure 1(a) at $\sigma = \Delta P_T - \Delta P_\gamma$ if $\Delta P_\gamma > 0$, *i.e.*, if the liquid does not wet the porous material, as is generally the case in metal matrix composite infiltration (if $\Delta P_\gamma < 0$, the preform is further compressed right behind the infiltration front).

At the same time, heat exchange takes place between the preform and liquid metal, and solid metal forms at the infiltration front. When the temperature of the incoming metal is above T_m, a remelted zone is formed, which extends between x_s and x_e (Figure 1(b)).

From behind the infiltration front to the preform entrance, the liquid pressure increases from $\Delta P_\gamma + P_g$ to $\Delta P_T + P_g$. The effective stress, therefore, decreases, so that the preform relaxes behind the infiltration front.

C. *Fluid and solid mechanics*

For simplicity, we focus from the onset on one-dimensional infiltration along the x direction (three-dimensional generalization of governing equations is fairly trivial, as noted in References 3 and 56) and use the stationary x-axis defined previously. Darcy's law dictates that

$$u_l - u_s = -\frac{K}{(1 - V_{sf})\,\mu}\frac{\partial P}{\partial x} \qquad [2]$$

where u_l is the (positive) average local velocity of the liquid within the pores, u_s is the (negative) local velocity of the solid, K (a function of V_{sf}) is the permeability of the porous medium in ΔV, μ is the liquid viscosity, and P is the pressure in the liquid.

Mass conservation in the solid and liquid phases, respectively, dictates that

$$\frac{\partial V_{sf}}{\partial t} + \frac{\partial (V_{sf}\,u_s)}{\partial x} = 0 \qquad [3]$$

and that

$$-\frac{\partial V_{sf}}{\partial t} + \frac{\partial ((1 - V_{sf})\,u_l)}{\partial x} = 0 \qquad [4]$$

Finally, having neglected inertial and body forces in both solid and liquid, stress equilibrium dictates that

$$\frac{\partial P}{\partial x} = -\frac{\partial \sigma}{\partial x} \qquad [5]$$

where σ is the effective stress acting in the solid along x, counted as positive in compression and averaged over a surface area comprising both solid and liquid.

D. *Heat Transfer*

As in infiltration of a nondeformable preform by pure metal,[3] when the preform temperature is below the matrix melting point and the superheat ($T_o - T_m$) is not too large, a region where solid and liquid metal coexist forms behind the infiltration front (called region 1, as in Reference 3). Maintaining the assumptions made in Reference 3 that the interface between the solid and liquid matrix material is at

equilibrium everywhere and that the influence of capillary forces on the metal melting point can be neglected, the temperature remains fixed at T_m where solid matrix is present.

Superheated metal entering the preform will remelt the solid metal formed at the infiltration front, leading to the formation of a remelted zone comprising only liquid matrix and fibers (region 3 in Figure 1 of Reference 3). Within a volume element ΔV in this region, the heat-transfer equation is written as

$$\frac{\partial}{\partial x} \cdot \left(k_c \frac{\partial T}{\partial x} \right) = \rho_c c_c \frac{\partial T}{\partial t} + \left(\rho_m c_m (1 - V_f) u_1 + \rho_f c_f V_f u_s \right) \cdot \frac{\partial T}{\partial x} \quad [6]$$

where k_c is the thermal conductivity of the composite, ρ is the density, c is the heat capacity, and subscripts c, m, and f, refer to the composite, matrix, and fibers, respectively. The values of k_c and c_c are estimated as in Reference 3 and are functions of V_f.

Given that the local permeability within the remelted zone is far higher than that in the upstream region containing solid metal, the pressure gradient is shallow in the remelted region, so that the fluid pressure remains close to P_o. In what follows, we therefore make the simplification that, everywhere within the remelted region, $P = P_o = \Delta P_T + P_g$ and $V_f = V_f^r$, V_f^r corresponding to $\sigma = 0$ on the unloading portion of the stress-strain curve.

E. *Inter-Region Boundary Equilibria*

Mass and energy conservation must be obeyed at moving boundaries separating the different regions. We neglect heat transfer in the (generally poorly conducting) fiber preform ahead of the infiltration front. The main equations are, then, as follows (*cf.* References 3 and 56 for a more complete description):

- At the infiltration front, $x = x_f$

$$P = P_g + \Delta P_\gamma \quad [7]$$

$$T = T_m \quad [8]$$

$$\rho_m \Delta H V_s = \rho_f c_f V_f (T_m - T_f) \quad [9]$$

$$V_f = V_f^i \quad [10]$$

$$u_s = u_1 \frac{V_f^c - V_f^i}{V_f^c} \quad [11]$$

- At the remelting front, $x = x_s$

$$P(x_s^-) = P(x_s^+) \quad [12]$$

$$T(x_s^-) = T(x_s^+) = T_m \quad [13]$$

$$-\left(k_c \frac{\partial T}{\partial x}\right)_{x_s^-} = \rho_m \Delta H V_s \frac{\partial x_s}{\partial t} \quad [14]$$

$$(1 - V_f(x_s^-)) u_l(x_s^-) = (1 - V_{sf}(x_s^+)) u_l(x_s^+) + V_s(x_s^+) u_s(x_s^+) \quad [15]$$

$$V_f(x_s^-) u_s(x_s^-) = V_f(x_s^+) u_s(x_s^+) \quad [16]$$

where ΔH is the enthalpy of fusion of the metal.

III. SOLUTION METHODOLOGY

A. *Lower- and Upper-Bound Estimation of the Infiltration Rate*

When solid metal forms during infiltration, the stress-strain curve of the preform containing solid metal can no longer be expected to coincide with that of the dry preform. This introduces a significant complication in prediction of infiltration kinetics, since the rheology of the solid phase must be known for an exact solution of the problem to be derivable and since, where solid metal is present, this rheology is both difficult to measure (particularly for all possible amounts of solid formed) and likely to be strongly time-dependent. To approach the solution, we therefore consider two limiting cases which provide bounds for the local preform strain and, hence, for the rate of infiltration. These bounds describe the greatest and the least possible extent of preform relaxation.

(1) An upper bound for the infiltration rate is obtained by assuming that the solid metal present exerts no influence on the stress-strain behavior of the preform. The compressive strain on the porous medium, therefore, decreases along the preform toward its entrance, along the stress-strain curve for unloading, from $\sigma = \Delta P_T - \Delta P_\gamma$ to $\sigma = 0$ (Figure 1(a)). Since the solid metal remains attached to the preform and moves locally with it, V_s is always locally related to V_f through Eq. [58] of Reference 3,

$$V_s = \frac{(T_m - T_f) \rho_f c_f V_f}{\rho_m \Delta H} \quad [17]$$

(2) A lower bound for the infiltration rate is obtained by assuming that solid metal locks the preform in its initial, most fully compressed state, wherever solid metal is present, at $V_f = V_f^i$.

These conditions represent, respectively, an upper and a lower bound on the infiltration rate, because solid metal will always impede preform relaxation and, hence, prevent an increase in preform permeability. These bounds are, furthermore, mathematically convenient because the preform rheology is, for each extreme, everywhere independent of time. This, in turn, allows use of the Boltzmann transformation for simultaneous solution of all the governing equations.

B. *The Boltzmann Transformation*

When considering each of these bounds, the set of Eqs. [2] through [6] can be transformed as in Reference 56 into ordinary differential equations using the Boltzmann transformation. To this effect, we define χ as

$$\chi = \frac{(x - x_e)}{\psi \sqrt{t}} \quad [18]$$

where x_e is the position of the porous preform entrance at time t. Because the preform relaxes, $x_e < 0$. The scalar ψ

is chosen such that the position of the infiltration front corresponds to $\chi = 1$;

$$L = \psi \sqrt{\bar{t}} \qquad [19]$$

where L is the total length of the infiltrated portion of the preform, as shown in Figure 1(b). Functions $l(\chi)$ and $s(\chi)$ are defined by

$$u_1 = \frac{\psi\, l\,(\chi)}{2\sqrt{\bar{t}}} \qquad [20]$$

$$u_s = \frac{\psi\, s\,(\chi)}{2\sqrt{\bar{t}}} \qquad [21]$$

Using this transformation, Eqs. [2] through [6] become a set of nonlinear ordinary first-order differential equations which can be solved numerically, along with the boundary conditions [8] through [16].

C. *The Approximate Solution*

For the isothermal infiltration of a deformable porous medium,[56] a far simpler approximate solution of the fluid flow equations can be obtained by considering the average local velocity of the solid porous medium to be significantly smaller throughout than the average local liquid velocity: $(-u_s) \ll u_l$. With this assumption, the infiltration rate constant ψ is obtained directly using a straightforward numerical integration. As discussed in Reference 56, this solution is not rigorous because it violates conservation of volume; however, this approximation was shown, for isothermal infiltration, to yield results which are quite close to those of the full analysis, with far greater computational simplicity. The underlying reason for this is that the approximation made is most inconsequential where the preform is most compressed, *i.e.*, right behind the infiltration front; this is precisely the ''bottleneck'' which governs the rate of infiltrant flow.

In what follows, we will first extend the validity of this approximation for infiltration in the presence of matrix solidification, using the (computationally simpler) case of nonisothermal infiltration with no metal superheat. We will then use this solution in our analysis of the influence of metal superheat on infiltration kinetics.

IV. PREDICTION OF INFILTRATION KINETICS

A. *Infiltration with no Metal Superheat: $T_o = T_m$ and $x_s = x_e$*

1. *Upper-bound solution: full preform relaxation*

a. *Complete solution*

Transformation of Eqs. [2] through [5] is identical to that presented in Reference 56, with parameter θ of Reference 56 equal to $(1 - V_f - V_s)$, with V_s given by Eq. [17] and

$$D\,(\theta) = D\,(V_f) = K\,(V_{sf})\,\frac{\partial \sigma}{\partial V_f}$$

Eqs. [2] through [5] (which correspond to Eqs. [17] through [19] of Reference 56) then become

$$V_f'\,(\chi) = \frac{(l - s)\,(1 - V_f - V_s)\,\mu\,\psi^2}{2\,D(V_f)} \qquad [22]$$

$$s'\,(\chi) = [s(\chi) - \chi - s(0)]\left(\frac{-V_f'}{V_f}\right) \qquad [23]$$

$$l'\,(\chi) = [l(\chi) - \chi - s(0)]\left(\frac{V_{sf}'}{1 - V_{sf}}\right) \qquad [24]$$

where the prime symbol denotes derivation with respect to χ. The boundary conditions (Eqs. [20], [21], [25], and [26] in Reference 56) are

$$V_f = V_f^i \text{ at } \chi = 1^- \qquad [25]$$

$$V_f = V_f^r \text{ at } \chi = 0 \qquad [26]$$

$$s(\chi = 1^-) = [1 + s(0)]\,\frac{V_f^i - V_f^c}{V_f^i} \qquad [27]$$

and

$$1(\chi = 1^-) = [1 + s(0)]\,\frac{1 - V_f^i}{1 - V_{sf}^i} \qquad [28]$$

This set of nonlinear first-order equations is solved numerically for the parameter ψ and the functions $V_f(\chi)$, $l(\chi)$, and $s(\chi)$, using a midpoint Runge–Kutta scheme for integration[65] and a three-dimensional Newton–Raphson method to adjust the initial guesses of ψ^2, $l(\chi = 0)$, and $s(\chi = 0)$ for convergence, as in Reference 56.

b. *Simplified solution*

$(-u_s) \ll u_l$. The infiltration rate parameter ψ is now directly obtained by setting $V_f = V_f^r$ at $\chi = 0$ in the following equation (derived as in Reference 56):

$$\int_{V_{f(\chi)}}^{V_f^i} 2\,K_{(V_{sf})}\,\sigma'_{(V_f)}\,dV_f = (1 - V_f^i)\,\mu\,\psi^2\,(1 - \chi) \qquad [29]$$

and solving for ψ. The volume fraction and the effective stress can then be calculated as functions of χ by solving Eq. [29] again, but for an arbitrary χ.

2. *Lower bound: no preform relaxation*

In this case, solid metal prevents the preform from relaxing, and V_f is, everywhere, V_f^i. Governing and boundary equations then simply reduce to the equations of Reference 3 for the case of no metal superheat, and the rate of infiltration, measured by the parameter ψ, is given by

$$\psi^2 = \frac{2\,(\Delta P_T - \Delta P_\gamma)\,K(V_{sf}^i)}{\mu\,(1 - V_f^i)} \qquad [30]$$

B. *Influence of Metal Superheat*

We now consider the case where $T_o > T_m$, so that there is a region of $x_e < x < x_s$, as in Figure 1(b), where solid metal formed initially upon contact with the fibers has remelted. We assume that the temperature at $x = x_e$ is T_o at all times and, as indicated in Section II–D, we assume that $P = P_o$ and $V_f = V_f^r$ for $x_e < x < x_s$.

1. *Upper bound*

Solid metal present between x_s and x_f is considered not to affect relaxation of the porous medium, and we use the

simplified solution described in Section III–C, considering $u_s \cong 0$ in the region where solid metal is present. Setting $\Delta_{\chi f} = x_f/\psi\sqrt{t}$, $\Delta_{\chi e} = x_e/\psi\sqrt{t}$, and $\Delta_{\chi s} = x_s/\psi\sqrt{t}$, the following relations are obtained:

- from Eqs. [18] and [19], $\Delta_{\chi f} - \Delta_{\chi e} = 1$, and
- from Eq. [18], $\chi_s = \Delta_{\chi s} - \Delta_{\chi e}$.

Boundary conditions [25] and [26] are still valid, and [28] becomes

$$l\,(\chi = 1^-) = \frac{1 - V_f^i}{1 - V_{sf}^i} \qquad [31]$$

The boundary condition at $\chi = \chi_s$ is given by Eqs. [12] through [16]. Eq. [14] becomes

$$-2\,k_c T'\,(\chi s) = \rho_m\,\Delta H\,V_{sf}^r\,\psi^2\,\Delta_{\chi s} \qquad [32]$$

Since V_f remains constant within the remelted zone, the solid velocity at x_s is the same as that for $x = x_e$, so

$$s(\chi s^-) = \Delta_{\chi e} \qquad [33]$$

Since the preform relaxes fully, there is no discontinuity in preform volume fraction at the remelting front; hence, $V_f\,(\chi_s^-) = V_f\,(\chi_s^+)$, and, from Eq. [16], $s(\chi_s^-) = s(\chi_s^+)$. Eq. [15] then yields

$$\begin{aligned}(1 - V_f^r)\,[l\,(\chi_s^-) - l\,(\chi_s^+)] \\ + V_s^r\,[l\,(\chi_s^+) - s\,(\chi_s^+)] = 0\end{aligned} \qquad [34]$$

In region 1, where solid and liquid metal coexist $T = T_m$, Eqs. [2] and [5] imply that

$$l(\chi) = \frac{2\,K\,(V_{sf})}{(1 - V_{sf})\,\mu\,\psi^2}\,\frac{d\sigma}{dV_f}\,V_f' \qquad [35]$$

and, as in the previous case, Eqs. [3] and [4] yield

$$(1 - V_{sf})\,l(\chi) = (1 - V_f^i) = (1 - V_{sf}^r)\,l(\chi_s^+) \qquad [36]$$

Hence, the following relationship between χ and ψ is obtained, valid as well for $\chi = \chi_s$ and $V_f = V_f^r$:

$$\begin{aligned}\int_{V_{f(\chi)}}^{V_f^i} 2\,K\,(V_{sf})\,\frac{d\sigma}{dV_f}\,dV_f \\ = (1 - V_f^i)\,(1 - \chi)\,\mu\,\psi^2\end{aligned} \qquad [37]$$

In region 3, where superheated metal has remelted the solid present, using Eqs. [15] and [33], we have

$$l(\chi_s^-) = \Delta_{\chi e} + \frac{1 - V_f^i}{1 - V_f^r} \qquad [38]$$

which yields, by insertion into Eq. [6],

$$\frac{-2\,k_c T''}{\rho_c^r\,c_c^r\,\psi^2} = (\chi - \beta)\,T' \qquad [39]$$

with

$$\beta = \Delta_{\chi e} + \frac{\rho_m\,c_m\left\{(1 - V_f^i) + (1 - V_f^r)\,V_s^r\,\Delta_{\chi e}\right\} + \rho_f\,c_f\,V_f^r\,\Delta_{\chi e}}{\rho_c^r\,c_c^r} \qquad [40]$$

Equation [39] is solved between $\chi = 0$ ($T = T_o$) and $\chi = \chi_s$ ($T = T_m$), using an error function solution as in Reference 3, to yield the following temperature profile in region 3

$$\frac{T\,(\chi) - T_m}{T_0 - T_m} = \frac{\operatorname{erf}\left[\frac{\psi}{2\sqrt{\alpha_c^r}}\,(\chi - \beta)\right] - \operatorname{erf}\left[\frac{\psi}{2\sqrt{\alpha_c^r}}\,(\chi_s - \beta)\right]}{\operatorname{erf}\left[\frac{\psi}{2\sqrt{\alpha_c^r}}\,(-\beta)\right] - \operatorname{erf}\left[\frac{\psi}{2\sqrt{\alpha_c^r}}\,(\chi_s - \beta)\right]} \qquad [41]$$

where $\alpha_c^r = k_c^r/\rho_c^r c_c^r$. Finally, global conservation of fiber volume, between the initial compressed state and a relaxed state, yields

$$x_f\,V_f^i = (x_s - x_e)\,V_f^r + \int_{x_s}^{x_f} V_f\,(x)\,dx \qquad [42]$$

This equation can be written to give the value of $\Delta_{\chi f}$ as

$$\Delta_{\chi f} = 1 - \frac{1}{V_f^i}\int_{V_f^r}^{V_f^i} \chi\,(V_f)\,dV_f \qquad [43]$$

with $\chi(V_f)$ given from Eq. [37].

For a given set of parameters, a solution is easily found by an inverse method, which can then be used iteratively: first choose a value of χ_s, then evaluate ψ from Eq. [37], then calculate $\Delta_{\chi f}$ from Eq. [43], evaluating the function $\chi(V_f)$ from Eq. [37]. The values of $\Delta_{\chi e}$ and $\Delta_{\chi s}$ are then computed from Eqs. [18] and [19]. By then setting as equal the values of $T'(\chi_s)$ found from Eq. [32] and the derivative of Eq. [41], one calculates the corresponding value of T_m.

2. *Lower bound*

We now assume that solid metal locks the fibers in the compressed state corresponding to the pressure $\Delta P_T - \Delta P_\gamma$. Hence, for $\chi_s < \chi < 1$, $V_f(\chi) = V_f^i$. Equations describing the problem are very similar to those presented for case I: Eqs. [18], [19], [25], [26], [28], [32], [33], and [39] through [41] all remain unchanged. Equation [42] reduces to

$$(x_s - x_e)\,V_f^r = x_s\,V_f^i \qquad [44]$$

Equation [34] is different, as $s(\chi_s^+) = 0$, and becomes

$$(1 - V_f^r)\,l(\chi_s^-) + V_f^r\,s\,(\chi_s^-) = [1 - V_{sf}^i]\,1\,(\chi_s^+) \qquad [45]$$

The value of β, given by Eq. [40], therefore becomes

$$\beta = \Delta_{\chi e}\,(1 - \frac{V_f^i}{V_f^r})\,(2 - \frac{\rho_m\,c_m}{\rho_c^r\,c_c^r} + \frac{\rho_m\,c_m\,(1 - V_f^i)}{\rho_c^r\,c_c^r} \qquad [46]$$

The set of flow equations in region 1 is simply derived from Eq. [2] and from the first two terms of Eq. [36] $(1 - V_{sf})\,l(\chi) = 1 - V_f^i$, neglecting any pressure drop within region 3.

$$\psi^2 = \frac{-2\,K(V_{sf}^i)\,(\Delta P_T - \Delta P_\gamma)}{\mu\,(1 - V_f^i)\,(\Delta_{\chi f} - \Delta_{\chi s})} \qquad [47]$$

Once again, the solution is found by choosing a value of χ_s and deriving $\Delta_{\chi s}$, $\Delta_{\chi e}$, $\Delta_{\chi f}$, and ψ^2 successively and then by deriving T_m from Eqs. [32] and [41].

V. RESULTS AND DISCUSSION

As a practical example of an application of the present analysis, we consider the unidirectional infiltration of pure aluminum into a SAFFIL* δ-alumina preform, of initial

*SAFFIL is a trademark of ICI Americas, Inc., Wilmington, DE.

Table I. Values of Constants for Aluminum and SAFFIL[4,5]

Property	Units	Aluminum	SAFFIL
ρc	$(J \cdot K^{-1} \cdot m^{-3})$	$2.6 \cdot 10^6$	$4.0 \cdot 10^6$
$\rho_m \Delta H$	$(J \cdot m^{-3})$	$9.5 \cdot 10^8$	—
k	$(W \cdot m^{-3} \cdot K^{-1})$	93	8
α	$(m^2 \cdot s^{-1})$	$36 \cdot 10^{-6}$	$2 \cdot 10^{-6}$
μ	$(Pa \cdot s)$	$1.3 \cdot 10^{-3}$	—
σ_{LA}	$(J \cdot m^{-2})$	0.914	—
θ	(deg)	106	—
S_f	(m^{-1})	—	$-977{,}800 + 2.2217\ 10^7\ V_f$

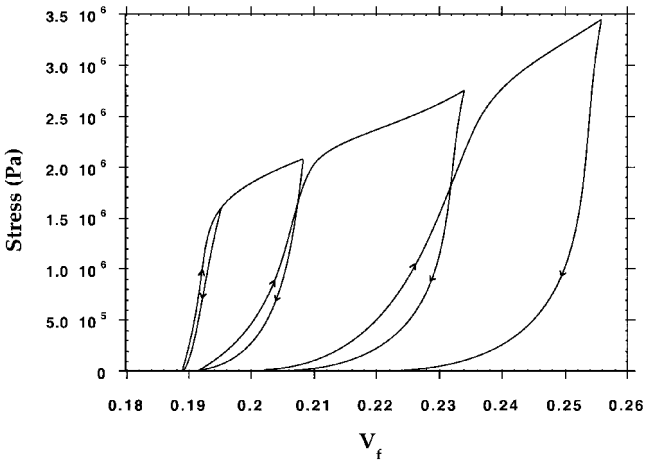

Fig. 2—Stress-strain curves for uniaxial cyclic compression of a dry SAFFIL preform, initial volume fraction $V_f = 0.188$, at $T_f = 150$ °C, with a maximum load of 3.45 MPa.

volume fraction $V_f = 0.188$, under constant applied pressure. The physical data relevant to this system are given in Table I. The infiltration direction is orthogonal to the fiber axis, and the function $K(V_{sf})$ is taken as in Reference 3, assuming that the solid metal forms as a sheath around the fibers and that the initial fiber radius (r_f) is equal to 2.72 μm. The terms ΔP_γ and S_f in Eq. [1] are functions of the fiber volume fraction $V_f(\Delta P_T)$ at the onset of infiltration; their dependence on V_f is estimated by linear interpolation of results given in Reference 5 for the range from 0.1 to 0.25 (Table I).

The relation between σ and V_f used in the calculations (with σ expressed in pascal) is given as follows.

(1)For the compression part of the curve,

$$V_{f\text{comp}}(\sigma) = a + b\,\sigma + c\,\sigma^2 + d\,\sigma^3 + e\,\sigma^4 + f\,\sigma^5, \quad \text{for } \sigma < 2.07 \text{ MPa, and} \quad [48]$$

$$V_{f\text{comp}}(\sigma) = g + h\,\sigma, \text{ for } \sigma > 2.07 \text{ MPa} \quad [49]$$

where $a = 0.18838$, $b = 5.3766\ 10^{-9}$,

$c = -3.966583\ 10^{-15}$, $d = 5.5275\ 10^{-21}$,

$e = -5.1431848\ 10^{-27}$, $f = 1.865145\ 10^{-33}$,

$g = 0.136477$, and $h = 3.47692\ 10^{-8}$.

(2) For relaxation after compression to P_a,

$$\sigma(V_f) = P_a\,(1 - (t + uA + vA^2 + wA^3)) \quad [50]$$

where $t = 0.027219$, $u = 55.4816$, $v = -1169.453$, $w = 8646.153$, and

$$A = \left(\frac{V_{f\text{comp}}(P_a) - V_f}{V_{f\text{comp}}(P_a) - 0.188} \right)^{1/3}$$

This expression is obtained from a curve fit of oedometer test (confined compression) data of a dry SAFFIL preform, at 423 K, with an initial volume fraction of 0.188 (Figure 2). These data were measured using an INSTRON* testing machine at a crosshead speed of 0.51 mm per minute (further details concerning the experimental procedure are given in Reference 66). The curves of σ vs V_f first exhibit a region of elastic deformation in which the apparent modulus is high and where unloading curves superimpose on loading curves. This is followed by a region of lower apparent modulus, in which unloading shows significant residual deformation of the preform. Irreversible deformation of the preforms is most likely caused by fiber and binder breakage, as well as fiber rearrangement, as proposed by Clyne and Mason.[59] Since none of the likely preform deformation mechanisms (elastic deformation, fiber breakage, and fiber rearrangement) are time-dependent, data from mechanical tests should accurately replicate the preform deformation experienced during infiltration, despite the much-higher strain rates imposed during infiltration. The observed stress-strain behavior is quite similar to that observed during oedometric compression of preconsolidated soils.[61] This probably results from the preform fabrication process, namely, compression of a water-based slurry containing the fibers and colloidal silica as a binder. We note that this behavior is different from the power-law behavior usually observed in compression experiments of unconsolidated long fibers or short-fiber mats also used in composite material processing.[67,68,69]

*INSTRON is trademark of Instron, Inc., Canton, MA.

Calculated values of ψ^2 are plotted in Figures 3 through 5, for the considered SAFFIL preform of initial $V_f = 0.188$ with no metal superheat, for plausible values of infiltration parameters. Three different calculations are plotted on each of these figures: curve a, obtained by assuming that the preform is incompressible; curve b, using the upper-bound solution; and curve c, using the lower-bound solution. In all cases, if ΔP_T is lower than the capillary pressure drop given in Eq. [1], no infiltration occurs. This determines the minimum threshold pressure found in Figures 3 and 4.

When neglecting preform compression (curve a), V_f stays constant at 0.188, and the infiltration rate parameter ψ^2 increases linearly with the applied pressure ΔP_T, with a slope of $2\ K(V_{sf})/\mu(1 - V_f)$, as derived in Reference 4. When preform compression is taken into account (curves b and c), ψ^2 deviates strongly from the linear behavior predicted with no preform compression. This is because an increase in applied pressure now activates the two competing mechanisms of (1) increased driving force and (2) reduced permeability due to preform compression. As the applied pressure is increased, the infiltration rate therefore increases up to a maximum, to decrease when preform deformation becomes predominant. The infiltration rate is found to drop to zero when V_{sf} reaches the packing density limit, at which point the solid phase completely blocks flow at the infiltra-

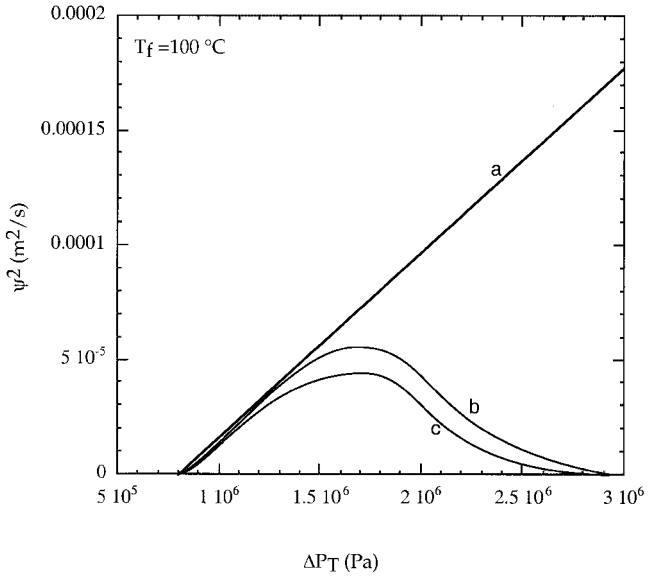

Fig. 3—Theoretical values of ψ^2 *vs* ΔP_T at T_F = 100 °C for infiltration with no superheat: (*a*) assuming that the preform does not compress; (*b*) upper-bound assuming that the solid metal surrounding the fibers leaves the mechanical relaxation of the preform unaffected; and (*c*) lower-bound assuming that the solid metal retains the preform everywhere to V_f^i corresponding to $\sigma = \Delta P_T - \Delta P_\gamma$.

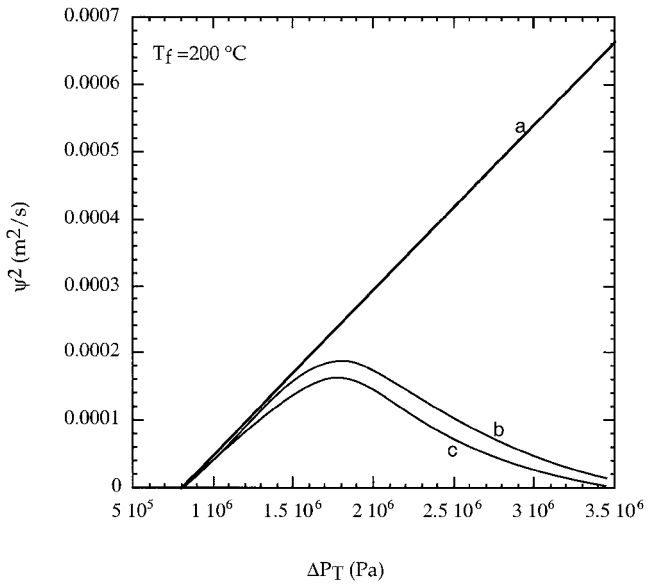

Fig. 4—Theoretical values of ψ^2 *vs* ΔP_T at T_F = 200 °C for infiltration with no superheat: (*a*) assuming that the preform does not compress; (*b*) upper-bound assuming that the solid metal surrounding the fibers leaves the mechanical relaxation of the preform unaffected; and (*c*) lower-bound assuming that the solid metal retains the preform everywhere to V_f^i corresponding to $\sigma = \Delta P_T - \Delta P_\gamma$.

tion front (where $K = 0$). From these figures, it appears clearly that an increase in applied pressure may not always result in a faster infiltration rate, that preform compression can even prevent infiltration altogether, and that there exists an optimal infiltration pressure in the presence of preform compression.

A second important result apparent in these curves is that the calculated upper and lower bounds are quite close to each other (for this system), especially if one keeps in mind that permeabilities and infiltration rates are seldom predicted with a precision better than a factor of 2. This indicates that one could bracket fairly accurately the range of infiltration kinetics for a given set of processing parameters, having only measured the dry preform compression behavior.

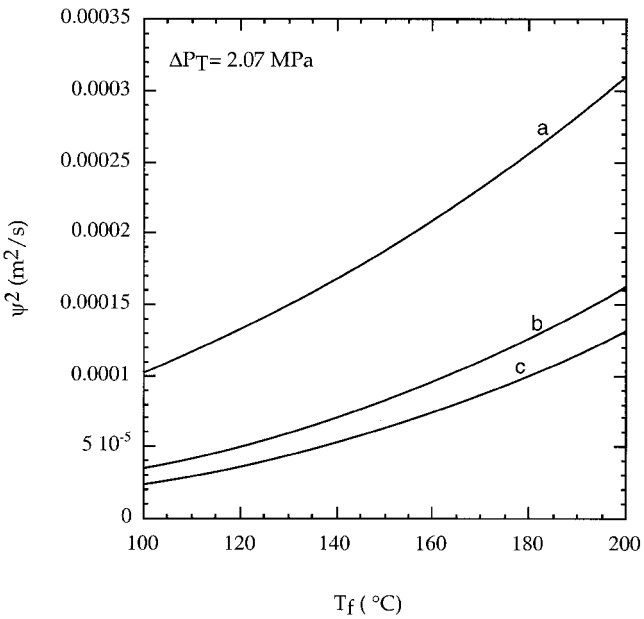

Fig. 5—Theoretical values of ψ^2 *vs* T_F for ΔP_T = 2.07 MPa for infiltration with no superheat: (*a*) assuming that the preform does not compress; (*b*) upper-bound assuming that the solid metal surrounding the fibers leaves the mechanical relaxation of the preform unaffected; and (*c*) lower-bound assuming that the solid metal retains the preform everywhere to V_f^i corresponding to $\sigma = \Delta P_T - \Delta P_\gamma$.

The value of the applied pressure corresponding to a maximal rate of infiltration shifts slightly to higher pressures when the preform temperature is increased (Figure 4), because less solid metal is formed. For a given applied pressure, an increase in preform temperature will, as expected, increase the rate of infiltration since less solid metal is present (Figure 5).

Results from the simplified solution of the upper-bound limit (crosses *i'*), are compared to results of the upper (curve i) and lower (curve ii) bounds in Figure 6, for conditions identical to those in Figure 3. It is seen that error induced from the approximate solution is very small, confirming the conclusion of Reference 56 that this solution, far more straightforward to compute, can give a good approximation of the infiltration kinetics for deformable preforms. This is also seen in Figure 7, which plots the distribution of V_f for typical infiltration conditions and no superheat, for the upper (curve i) and lower (curve ii) bounds and the simplified solution (crosses i'). For the upper bound and the simplified solutions, a similar distribution in volume fraction is obtained between V_f^i at the infiltration front and V_f^r at the preform entrance. This figure also shows that, if solid metal does not prevent relaxation of the preform (as in the upper-bound solution), a significant gradient in volume fraction fiber is obtained in the final, solidified composite material.

The effect of superheat ($\Delta T_s = T_o - T_M$) is presented in Figures 8 and 9, for typical infiltration parameters, for three conditions: (1) for the upper bound, using the simplified solution where solid metal is present and assuming that the preform is relaxed to V_f^r in the remelted zone; (2) for the

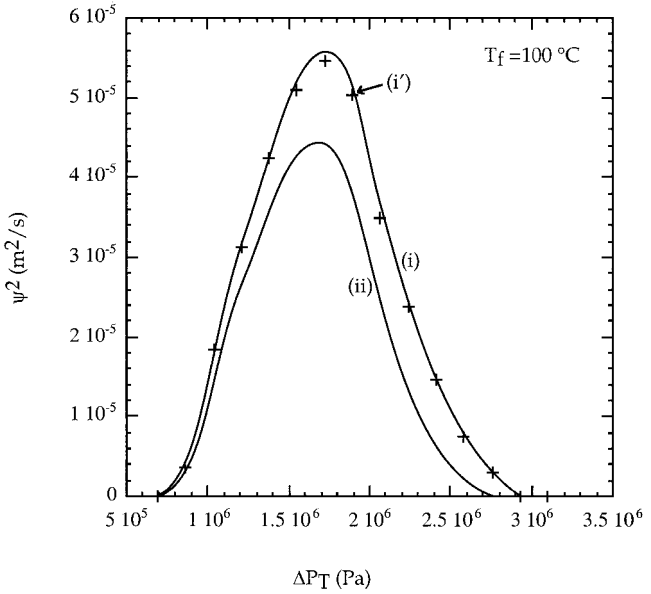

Fig. 6—Theoretical values of ψ^2 *vs* ΔP_T at T_F = 100 °C for infiltration with no superheat: (i) upper-bound assuming that the solid metal surrounding the fibers leaves the mechanical relaxation of the preform unaffected; (i') (crosses) approximate upper-bound solution calculated assuming that the velocity of the solid phase is negligible; and (ii) lower-bound assuming that the solid metal retains the preform everywhere to V_f^i corresponding to $\sigma = \Delta P_T - \Delta P_\gamma$.

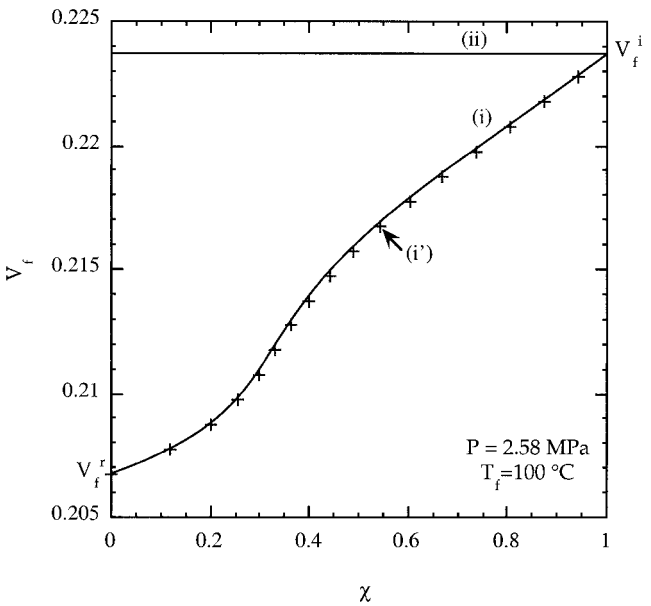

Fig. 7—Volume fraction profile along the length of a sample, for ΔP_T = 2.58 MPa, T_F = 100 °C, and no superheat: (i) upper-bound assuming that the solid metal surrounding the fibers leaves the mechanical relaxation of the preform unaffected; (i') (crosses) approximate upper bound solution calculated assuming that the velocity of the solid phase is negligible; (ii) lower-bound assuming that the solid metal retains the preform everywhere to V_f^i corresponding to $\sigma = \Delta P_T - \Delta P_\gamma$.

lower bound, with the fiber preform locked into the compressed state $V_f = V_f^i$ where solid metal is present and relaxed to V_f^r in the remelted zone; and (3) assuming that the preform remains compressed to V_f^i over the total length of the composite. The upper and lower bounds are once again close, although they tend to separate somewhat further for high amounts of superheat. As expected from previous results with no compression,[4] the effect of superheat on infiltration kinetics is rather small compared to that of preform initial temperature or volume fraction (Figure 5). This is because the superheat tends to remelt solid metal present at the gate region, but does not affect much the bottleneck region, located near the infiltration front, in which the fraction solid is high and the local permeability low. The influence of superheat on the length of the remelted zone is strong (Figure 9); this effect can be significant for compressible preforms, since it affects the volume fraction distribution in the composite produced.

Simple calculations, as derived in Reference 3, were used

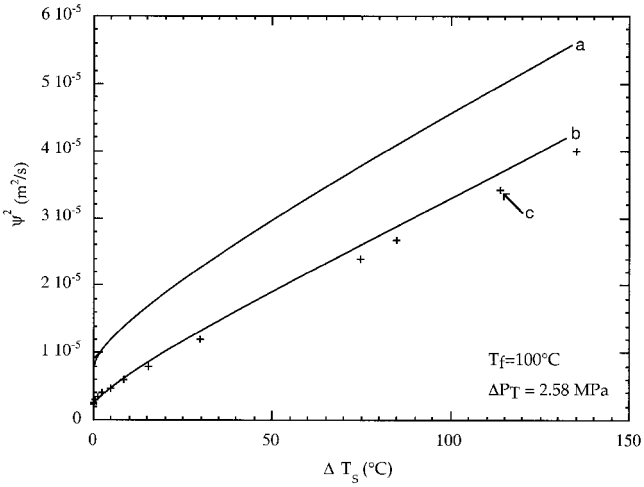

Fig. 8—Theoretical values of ψ^2 *vs* amount of superheat ΔT_S for ΔP_T = 2.58 MPa and T_F = 100 °C: (*a*) upper bound, solid metal leaving mechanical relaxation of the preform unaffected; (*b*) lower bound, solid metal where present retaining the preform volume fraction at V_f^i and with full preform relaxation elsewhere; and (*c*) assuming that the preform is everywhere compressed to V_f^i.

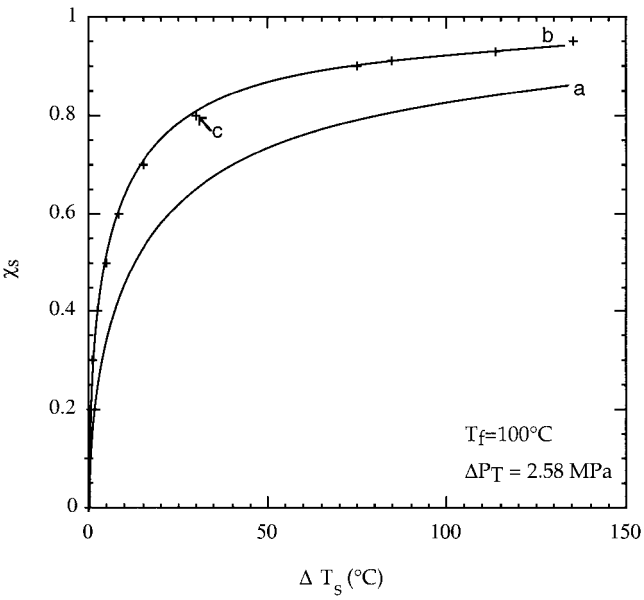

Fig. 9—Theoretical values of χ_s *vs* amount of superheat ΔT_S for ΔP_T = 2.58 MPa and T_F = 100 °C: (*a*) upper bound, solid metal leaving mechanical relaxation of the preform unaffected; (*b*) lower bound, solid metal where present retaining the preform everywhere to V_f^i and with full preform relaxation elsewhere; and (*c*) assuming that the preform is everywhere compressed to V_f^i.

to derive the infiltration rate for a constant volume fraction of fibers (condition c), neglecting the effect of relaxation within the remelted zone. This calculation is not rigourous, as the boundary condition $V_f = V_f^r$ for $\chi = 0$ is not respected, but leads to only a slight underestimation of the lower bound. This result confirms that infiltration kinetics are not strongly influenced by the value of the volume fraction fiber within the remelted region (as the relaxation of the fiber preform is not very extensive) and justifies the assumption of a uniform volume fraction in the remelted region, which was used for the upper- and lower-bound calculations. This result also justifies the use of such a simple method as a first approximation of the influence of superheat on the size of the remelted region and on volume fraction fiber distribution: satisfactory agreement was reported in Reference 21 between experimental results from die-casting experiments and a similar analytical approach.

In summary, for the practical case explored here at least, upper and lower bounds on the one hand, and rigorous and simplified approaches on the other, all yield relatively similar results. The significant influence exerted by preform compression on infiltration rate can, therefore, be analyzed with relative simplicity and precision using the simplifications and the bounding approach proposed here. The underlying reason for this conclusion is, in all cases, the fact that the rate of flow is determined mostly by the bottleneck region located right behind the infiltration front and that, as long as the slug-flow assumption remains valid, this bottleneck is described with relatively good precision when simplifications proposed here are used.

The final distribution of reinforcement found in the composite is, however, more strongly dependent on the influence exerted by solid metal on preform relaxation: a nonrelaxed and a fully relaxed preform will show significantly different fiber distributions, particularly if relaxation continues after cessation of flow. Fiber distributions found in References 21 and 22 indicate that, in squeeze casting at least, process times are sufficiently short for solid metal to hinder fiber preform relaxation significantly. This, in turn, indicates that, for this relatively rapid infiltration process at least, reality is more closely described by the present lower bound.

VI. CONCLUSIONS

The infiltration rate and fiber volume fraction distribution, during slug-flow infiltration of a deformable porous medium in the presence of matrix solidification, are predicted using a bounding approach. The approach is motivated by the fact that the influence of matrix partial solidification on the rheological behavior of the porous preform is, in general, hard to predict or to measure. The upper bound for the infiltration rate assumes that solid metal exerts no influence on preform relaxation, while the lower bound assumes that solid metal confers complete rigidity to the preform, which, thus, remains compressed under the externally applied pressure minus the capillary pressure drop. A full solution of the governing equations is given for the case where a constant pressure differential drives the fluid flow, using the Boltzmann transformation.

A simplified approach for the upper bound is also proposed, based on the assumption that the solid velocity can be neglected throughout in favor of the liquid velocity. The influence of superheat within the infiltrating metal is also addressed, using the simplified solution and neglecting the pressure drop in the remelted region.

Application of this analysis to the infiltration of short-fiber preforms by pure aluminum shows that compression of the fiber preform causes the infiltration rate to deviate strongly from that which is calculated by assuming that the preform is rigid. The predicted rate of infiltration increases with applied pressure to a maximum, then decreases significantly, leading eventually to complete blockage of flow. The upper- and lower-bound solutions are close and, thus, provide brackets for the infiltration-rate parameter which are well within the usual experimental scatter. Moreover, the proposed simplified solution agrees well with the upper-bound solution and, hence, provides a far-simpler method to compute this bound.

Superheat in the infiltrating metal is shown to exert only a minor effect on infiltration kinetics, a result that is consistent with the case of a rigid preform. Its effect on the length of the remelted region is, however, significant; hence, superheat can influence the final reinforcement distribution in the composite when matrix solidification prevents preform relaxation significantly. This is, indeed, observed in squeeze-cast aluminum matrix composites.

An important overall conclusion that emerges from this work is that the relatively high analytical complexity of the problem at hand can be reduced significantly using simplifications explored in this work. These simplifications consist of initially (1) neglecting the solid-phase velocity in favor of that of the liquid, and (2) considering the melt superheat to be zero. With these assumptions, bounds on the infiltration rate become relatively simple to calculate with good precision. The underlying reason for this is that the region near the infiltration front, which serves as a bottleneck for flow, remains well described for both bounds with these assumptions. In general, it is expected that the two bounds will be close; hence, this approach should allow fairly precise prediction of the infiltration rate and of the optimal applied pressure for rapid infiltration. Then, with the infiltration rate thus estimated, bounds (corresponding to the same limits for the influence of solid metal on preform deformation, but which will generally not be close) can be proposed for the distribution of reinforcement volume fraction in the composite during, and after, infiltration. To this end, the influence of melt superheat must be taken into account in the lower-bound calculation, because this parameter exerts a significant influence on the reinforcement distribution; however, the calculation remains simple.

ACKNOWLEDGMENTS

We gratefully acknowledge sponsorship of this work by ALCOA under the supervision of Dr. Warren Hunt.

APPENDIX: GLOSSARY

ΔP_γ	capillary pressure drop (Pa)
ΔP_T	applied pressure (Pa) $= P_o - P_g$
ΔV	representative volume element (m^3)
$\Delta_{\chi f}$	$= x_f/\psi\sqrt{\underline{t}}$
$\Delta_{\chi e}$	$= x_e/\psi\sqrt{\underline{t}}$
$\Delta_{\chi s}$	$= x_s/\psi\sqrt{t}$

μ	liquid viscosity (Pa·s)
ψ	kinetics parameter, such that $L = \psi\sqrt{t}$
$\rho_c\ c_c$	volumetric heat capacity of the composite ($J{\cdot}K^{-1}{\cdot}m^{-3}$)
$\rho_m\ c_m$	volumetric heat capacity of the matrix ($J{\cdot}K^{-1}{\cdot}m^{-3}$)
$\rho_m\ \Delta H$	volumetric latent heat of solidification of the metal ($J{\cdot}m^{-3}$)
σ	*effective* stress (Pa)
σ_{LA}	liquid matrix surface energy ($J{\cdot}m^{-2}$)
θ	contact angle of the liquid metal on the flat, solid substrate material
χ	fractional distance along the composite
K	permeability tensor of the porous medium (m^2)
k_c	thermal conductivity of the composite ($W{\cdot}m^{-1}{\cdot}K^{-1}$)
L	total length of the infiltrated portion of the preform (m)
$l_{(\chi)}$	reduced liquid-phase velocity
P	local pressure in the liquid (Pa)
P_g	gas pressure (Pa)
P_o	total applied pressure (Pa)
S_f	total surface area of solid/liquid interface per unit volume of matrix (m^{-1})
$s(\chi)$	reduced solid-phase velocity
t	time (s)
T_f	initial preform temperature (K)
T_m	metal melting temperature (K)
T_o	initial metal temperature (K)
u_l	(positive) average local velocity of the liquid within the pores ($m{\cdot}s^{-1}$)
u_s	(negative) local velocity of the solid ($m{\cdot}s^{-1}$)
V_f	local fiber volume fraction
V_f^c	fiber volume fraction corresponding to $\sigma = \Delta P_T$
V_f^i	fiber volume fraction corresponding to $\sigma = \Delta P_T - \Delta P_\gamma$
V_f^r	fiber volume fraction corresponding to $\sigma = 0$
V_s	volume fraction of the solid metal phase
V_{sf}	volume fraction of all solid phases (fiber + metal)
x	position (m)
x_e	position of the porous preform entrance at time t (m)
x_s	position of the remelting front at time t(m)

REFERENCES

1. A. Mortensen, V.J. Michaud, and M.C. Flemings: *J. Met.*, 1993, vol. 45, pp. 36-43.
2. A. Mortensen and I. Jin: *Int. Mater. Rev.*, 1992, vol. 37, pp. 101-28.
3. A. Mortensen, L.J. Masur, J.A. Cornie, and M.C. Flemings: *Metall. Trans. A*, 1989, vol. 20A, pp. 2535-47.
4. L.J. Masur, A. Mortensen, J.A. Cornie, and M.C. Flemings: *Metall. Trans. A*, 1989, vol. 20A, pp. 2549-57.
5. A. Mortensen and T. Wong: *Metall. Trans. A*, 1990, vol. 21A, pp. 2257-63.
6. R.B. Calhoun and A. Mortensen: *Metall. Trans. A*, 1992, vol. 23A, pp. 2291-99.
7. V.J. Michaud, L. Compton, and A. Mortensen: *Metall. Mater. Trans. A*, 1994, vol. 25A, pp. 2145-52.
8. T.G. Gutowski, T. Morigaki, and Z. Cai: *J. Comp. Mater.*, 1987, vol. 21, pp. 172-188.
9. R. Dave: *J. Comp. Mater.*, 1990, vol. 24, pp. 23-41.
10. L. Trevino, K. Rupel, W.B. Young, M.J. Liou, and L.J. Lee: *Polym. Comp.*, 1991, vol. 12, pp. 20-29.
11. G.D. Smith and A. Poursartip: *J. Comp. Mater.*, 1993, vol. 27, pp. 1695-1711.
12. T. Imai, Y. Nishida, M. Yamada, H. Matsubara, and I. Shirayanagi: *J. Mater. Sci. Lett.*, 1987, vol. 6, pp. 343-45.
13. Y. Nishida, H. Matsubara, M. Yamada, and T. Imai: *4th Japan–U.S. Conf. on Composite Materials*, Proc. Conf., Washington, DC, 1988, Technomic Publishing Co., Lancaster - Basel, pp. 429-38.
14. B.R. Henriksen and T.E. Johnsen: *Mater. Sci. Technol.*, 1990, vol. 6, pp. 857-861.
15. N.W. Rasmussen, P.N. Hansen, and S.F. Hansen: *Mater. Sci. Eng.*, 1991, vol. A135, pp. 41-43.
16. N.W. Rasmussen, P.N. Hansen, and S.F. Hansen: *Metal Matrix Composites—Processing, Microstructure and Properties, 12th Risø Int. Symp. on Materials Science*, Proc. Conf., Risø, Denmark, 1991, N. Hansen, D. Juul-Jensen, T. Leffers, H. Lilholt, T. Lorentzen, A.S. Pedersen, O.B. Pedersen, and B. Ralph, eds. Risø National Laboratory, Roskilde, Denmark, pp. 617-20.
17. H. Fukunaga: *Int. Symp. on Advances in Cast Reinforced Metal Composites*, Proc. Conf., Chicago, IL, 1988, S.G. Fishman and A.K. Dhingra, eds., ASM INTERNATIONAL, Metals Park, OH, 1988, pp. 101-07.
18. F. Kloucek and R.F. Singer: *Materials Science for the Future: 31st Int. SAMPE Symp. and Exhibition*, Proc. Conf., Los Angeles, CA, 1986, J.L. Bauer and R. Dunaetz, eds., SAMPE, Covina, CA, pp. 1701-12.
19. K. Ban, T. Arai, T. Sakakibara, and N. Miyake: U.S. Patent 4,506,721, 1985.
20. R.M. Andrews and A. Mortensen: *Metall. Trans. A*, 1991, vol. 22A, pp. 2903-15.
21. P. Jarry, V.J. Michaud, A. Mortensen, A. Dubus, and R. Tirard-Collet: *Metall. Trans. A*, 1992, vol. 23A, pp. 2281-89.
22. T. Yamauchi and Y. Nishida: *Acta Metall. Mater.*, 1995, vol. 43, pp. 1313-21.
23. C.G. Kang and G.S. Ku: *J. Comp. Mater.*, 1995, vol. 29, pp. 444-62.
24. D.A. Kenyon: *Bull. Math. Biology*, 1979, vol. 41, pp. 79-90.
25. R.F. Fisher: *Proc. R. Soc. London*, 1982, vol. B216, pp. 475-96.
26. R.F. Fisher: *J. Phys.*, 1988, vol. 406, pp. 1-14.
27. M. Klanchar and J.M. Tarbell: *Bull. Math. Biology*, 1987, vol. 49, pp. 651-69.
28. Y. Lanir: *Biorheology*, 1987, vol. 24, pp. 173-87.
29. S.J. Lai-Fook: *J. Appl. Physiol.*, 1988, vol. 64, pp. 2372-80.
30. G.B. Robinson and H.A. Walton: *Microvasc. Res.*, 1989, vol. 38, pp. 36-48.
31. M.K. Kwan, W.M. Lai, and V.C. Mow: *J. Biomech.*, 1990, vol. 23, pp. 145-55.
32. M.H. Holmes and V.C. Mow: *J. Biomech.*, 1990, vol. 23, pp. 1145-56.
33. S.I. Barry and G.K. Aldis: *J. Biomech.*, 1990, vol. 23, pp. 647-54.
34. D.R. Scott: *J. Geophysical Res.*, 1988, vol. 93, pp. 6451-62.
35. M. Spiegelman: *J. Fluid Mech.*, 1993, vol. 247, pp. 17-38.
36. J.R. Philip: *Water Resources Res.*, 1969, vol. 5, pp. 1070-77.
37. G.I. Barenblatt, V.M. Entov, and V.M. Ryzhik: *Theory of Fluid Flows through Natural Rocks*, Kluwer Academic Publishers, Dordrecht, The Netherlands, 1990, p. 395.
38. J. Bear: *Dynamics of Fluids in Porous Media*, American Elsevier, New York, NY, 1972, p. 206.
39. J. Bear and Y. Bachmat: *Introduction to Modeling of Transport Phenomena in Porous Media*, Kluwer Academic Publishers, Dordrecht, The Netherlands, 1990, p. 305.
40. V.N. Nikolaevskij: *Mechanics of Porous and Fractured Media*, World Scientific, Singapore, 1990, p. 472.
41. R.W. Lewis and B.A. Schrefler: *The Finite Element Method in the Deformation and Consolidation of Porous Media*, John Wiley & Sons, Chichester, United Kingdom, 1987, p. 344.
42. A.E. Scheidegger: *The Physics of Flow through Porous Media*, 3rd ed., University of Toronto Press, Toronto, 1974, p. 84.
43. Y. Lanir, S. Sauob, and P. Maretsky: *J. Appl. Mech.*, 1990, vol. 57, pp. 449-54.
44. K.H. Parker, R.V. Mehta, and C.G. Caro: *J. Appl. Mech.*, 1987, vol. 54, pp. 794-800.
45. G.S. Beavers and T.A. Wilson: *J. Appl. Mech.*, 1975, vol. 42, pp. 598-602.

46. G.S. Beavers, A. Hajii, and E.M. Sparrow: *J. Fluids Eng.*, 1981, vol. 103, pp. 432-39.
47. G.S. Beavers, K. Wittenberg, and E.M. Sparrow: *J. Fluids Eng.*, 1981, vol. 103, pp. 440-44.
48. M. Nazmi Sharabi: *J. Eng. Mech.*, 1984, vol. 110, pp. 1303-19.
49. P. Basak and M.R. Madhav: *J. Hydrogeology*, 1978, vol. 38, pp. 139-46.
50. G.W. Scherer: *J. Non-Cryst. Solids*, 1989, vol. 113, pp. 107-18.
51. R. Angulo, J.P. Gaudet, J.L. Thony, and M. Vauclin: *Comptes Rendus de l'Academie des Sciences de Paris*, 1990, vol. 310, pp. 341-45.
52. R. Angulo, J.P. Gaudet, J.L. Thony, and M. Vauclin: *Comptes Rendus de l'Academie des Sciences de Paris*, 1990, vol. 310, pp. 161-64.
53. T.N. Narasimhan and P.A. Witherspoon: *Water Resources Res.*, 1977, vol. 14, pp. 255-61.
54. T.N. Narasimhan and P.A. Witherspoon: *Water Resources Res.*, 1977, vol. 13, pp. 657-64.
55. X. Li, O.C. Zienkiewicz, and Y.M. Xie: *Int. J. Numer. Methods Eng.*, 1990, vol. 30, pp. 1195-1212.
56. J. Sommer and A. Mortensen: *J. Fluid Mech.*, 1996, vol. 311, pp. 193-217.
57. Y.W. Yang, G. Zografi, and E.E. Miller: *J. Colloid Interface Sci.*, 1988, vol. 122, pp. 35-46.
58. L. Preciozi, D.D. Joseph, and G.S. Beavers: *Int. J. Multiphase Flow*, 1996, vol. 22, pp. 1205-1222.
59. T.W. Clyne and J.F. Mason: *Metall. Trans. A*, 1987, vol. 18A, pp. 1519-30.
60. A. Mortensen: *Metall. Trans. A*, 1990, vol. 21A, p. 2287.
61. *Soil Mechanics*, T.W. Lambe and R.V. Whitman, eds., John Wiley & Sons, Inc., New York, NY, 1969.
62. M.K. Hubbert and W.W. Rubey: *J. Geological Soc. Am.*, 1959, vol. 70, pp. 115-66.
63. S.K. Garg and A. Nur: *J. Geophys. Res.*, 1973, vol. 78, pp. 5911-21.
64. A. Nur and J.D. Byerlee: *J. Geophys. Res.*, 1971, vol. 76, pp. 6414-19.
65. W.H. Press, B.P. Flannery, S.A. Teukolsky, and W.T. Vetterling: *Numerical Recipes: The Art of Scientific Computing (Fortran Version)*, Cambridge University Press, New York, NY, 1989.
66. J.L. Sommer: Ph.D. Thesis, Massachusetts Institute of Technology, Cambridge, MA, 1992.
67. Y.R. Kim, S.P. McCarthy, and J.P. Fanucci: *Polym. Comp.*, 1991, vol. 12, pp. 13-19.
68. S. Toll and J.-A.E. Manson: *6th Int. Conf. on Fibre Reinforced Composites*, Proc. Conf., Newcastle, 1994, Institute of Materials, London, 1994, pp. 25/1-25/10.
69. S. Toll and J.-A.E. Manson: *J. Appl. Mech.*, 1995, vol. 62, pp. 223-26.